The American Journal of Pathology, Vol. 175, No. 4, October 2009

DOI: 10.2353/ajpath.2009.090384

Tumorigenesis and Neoplastic Progression

Comparative Analysis of Metastasis Variants Derived from Human Prostate Carcinoma Cells

Roles in Intravasation of VEGF-Mediated Angiogenesis and uPA-Mediated Invasion

Erin M. Conn,* Kenneth A. Botkjaer,† Tatyana A. Kupriyanova,* Peter A. Andreasen,† Elena I. Deryugina,* and James P. Quigley*

From the Department of Cell Biology, The Scripps Research Institute, La Jolla, California; and the Department of Molecular Biology,† University of Aarhus, Aarhus, Denmark*

To analyze the process of tumor cell intravasation, we used the human tumor-chick embryo spontaneous metastasis model to select *in vivo* high (PC-hi/diss) and low (PC-lo/diss) disseminating variants from the human PC-3 prostate carcinoma cell line. These variants dramatically differed in their intravasation and dissemination capacities in both chick embryo and mouse spontaneous metastasis models. Concomitant with enhanced intravasation, PC-hi/diss exhibited increased angiogenic potential in avian and murine models. PC-hi/diss angiogenesis and intravasation were dependent on increased secretion of vascular endothelial growth factor (VEGF), since treating developing tumors with a function-blocking anti-VEGF antibody simultaneously inhibited both processes without affecting primary tumor growth. PC-hi/diss cells were also more migratory and invasive, suggestive of heightened ability to escape from primary tumors due to matrix-degrading activity. Consistent with this suggestion, PC-hi/diss cells produced more of the serine protease urokinase-type plasminogen activator (uPA) as compared with PC-lo/diss. The functional role of uPA in PC-hi/diss dissemination was confirmed by inhibition of invasion, angiogenesis, and intravasation with specific function-blocking antibodies that prevented uPA activation and blocked uPA activity. These processes were similarly sensitive to aprotinin, a potent inhibitor of serine proteases, including uPA-generated plasmin. Thus, our comparison of the PC-3 intravasation variants points to key roles for the uPA-plasmin system in PC-hi/diss intravasation, possibly via (1) promoting tumor cell matrix invasion and (2) facilitating development of VEGF-dependent angiogenic blood vessels. ***(Am J Pathol 2009, 175:1638–1652; DOI: 10.2353/ajpath.2009.090384)***

Subpopulations of congenic tumor cells differing in their metastatic potential, yet derived from the same parental cell line, have been invaluable in studying the complex process of metastasis.[1–6] Several approaches have been used to isolate subpopulations of tumor cells with different metastatic potentials and compare the resultant cell lines to identify key molecules functionally responsible for their respective metastatic abilities. Early studies using renal,[1] pancreatic,[2] prostate,[3] and colon[4] cancer cell lines demonstrated the possibility of generating metastatic variants from established tumor cell lines by *in vivo* selection. Modifications of these procedures have also been used to isolate cell variants with specific organ preferences for colonization after i.v. inoculation.[5,7] The murine experimental and spontaneous metastasis models used for *in vivo* selection often involve the detection and isolation of tumor cells from large overt metastases in lymph nodes, lungs, and other organs. This methodology is useful for generating populations of cells that have completed the later stages of the metastatic cascade (ie, vascular arrest, extravasation, and proliferation at the secondary site), but the selected cells do not necessarily

Supported by grants from the National Institutes of Health CA55852 and CA105412 (J.P.Q.), the National Cancer Institute T32CA77109-08 (E.M.C.), and by grants from the Danish National Research Foundation, the Danish Cancer Society, and the University of Aarhaus (P.A.A.).

Accepted for publication June 17, 2009.

Supplemental material for this article can be found on *http://ajp.amjpathol.org*.

Address reprint requests to Elena Deryugina, Ph.D. and James P. Quigley, Ph.D., The Department of Cell Biology, The Scripps Research Institute, 10550 North Torrey Pines Road, La Jolla, California 92037. E-mail: deryugin@scripps.edu; jquigley@scripps.edu.

differ in their capacity to accomplish early processes during cancer dissemination (ie, tumor cell escape, invasion, and intravasation). Isolating cell variants differing distinctly in their abilities to complete early rate-limiting steps in metastasis allows a more detailed and in depth investigation of the metastatic process. Selection and characterization of congenic *intravasation* variants can yield potentially important data on the specific molecular determinants of this greatly understudied individual step in the metastatic cascade.

The chick embryo spontaneous metastasis model provides a means to study tumor cell intravasation since tumor cells of many histological types form primary tumors when inoculated onto the highly vascularized chorioallantoic membrane (CAM).[8,9] Within 5 to 7 days, aggressive tumor cells enter the vasculature and can be detected in distal portions of the CAM, which serves as a repository of intravasated cells. Levels of tumor cell dissemination can be quantified by extracting genomic DNA from distal CAM tissue and amplifying primate-specific *Alu* DNA sequences using qPCR to determine actual numbers of human cells within a background of chicken tissue in vast cellular excess.[9,10]

By using the chick embryo spontaneous metastasis model, we have previously isolated *in vivo* intravasation variants from the HT-1080 human fibrosarcoma cell line.[9] The HT-1080 dissemination variants isolated using this system vary 50- to 100-fold in their ability to intravasate and metastasize to internal organs of the chick embryo. To better understand the molecular determinants of intravasation, these variants have been subjected in our laboratory to several types of analyses, including activity-based-protein profiling,[11] matrix metalloproteinase profiling,[12] and cell surface proteomics.[13] These investigations have implicated proteolysis in the intravasation processes and suggested contrasting roles for different matrix metalloproteinases in intravasation. The successful isolation of fibrosarcoma intravasation variants using the chick embryo spontaneous metastasis model suggested that cell variants differing specifically in their capacity to intravasate might also be isolated from other tumor types using a modification of this system.

Because carcinomas represent the majority of human cancers, we set out to select and characterize congenic carcinoma intravasation variants to elucidate mechanisms involved in early steps of carcinoma hematogenous metastasis. Our focus was on prostate carcinoma since this highly prevalent cancer is largely untreatable once metastasis occurs. The chick embryo spontaneous metastasis model was used for *in vivo* selection of dissemination variants from the well-characterized PC-3 prostate carcinoma cell line. Previously, PC-3 variants have been isolated from primary tumors and lymph node metastases of PC-3 tumor-bearing mice, suggesting the existence of cells with different metastatic potential.[3] We hypothesized that the chick embryo model would represent an alternative to the previously used selection strategies since it is uniquely well suited for *in vivo* selection of *intravasation* variants due to rapid recapitulation of the early stages of tumor cell dissemination, ie, escape from the primary tumor, entry into the vasculature, and arrest in the capillary network.[9]

In this study, we have established PC-3 carcinoma intravasation variants and subjected them to various *in vitro* and *in vivo* assays to analyze specific processes and molecules contributing to early metastatic dissemination. In particular, we analyzed tumor-induced angiogenesis to explore a potential link between increased tumor vascularity and early steps of tumor cell dissemination. In addition, adhesion, migration, and invasion characteristics were compared between the PC-3 cell dissemination variants to investigate the putative mechanisms involved in tumor cell escape. Finally, levels of specific angiogenic factors, epithelial to mesenchymal transition (EMT) associated proteins, and key proteases were compared between the prostate carcinoma cell variants. Potential roles of vascular endothelial growth factor (VEGF) and the serine protease urokinase-type plasminogen activator (uPA) were highlighted during these analyses. Based on the observations that these two molecules were differentially expressed between the PC-3 cell dissemination variants, we specifically modulated VEGF levels and uPA activity to further investigate their functional contributions to intravasation and dissemination of prostate carcinoma cells.

Materials and Methods

Chick Embryo Intravasation Assay

The PC-3 parental cell line was purchased from ATCC (Manassas, VA). PC-3 cells and subsequently isolated sublines were maintained in Dulbecco's modified Eagle's medium (DMEM) supplemented with 10% fetal bovine serum (Hyclone, Logan, UT) and 10 μg/ml gentamicin (D-10) in a humidified incubator at 37°C in the presence of 5% CO_2. For intravasation experiments, cells were passaged 48 hours before experiments, detached with trypsin/EDTA, washed in D-10, and resuspended in serum free DMEM (SF-DMEM) at a concentration of 8×10^7 cells per ml. SPAFAS White Leghorn embryos (Charles River, North Franklin, CT) were allowed to develop at 37°C in a humidified rotary incubator. On day 10 of incubation, a portion of the CAM was dropped by applying suction through a small hole in the air sac, essentially as described,[9,10] and 2×10^6 PC-3 cells in 25 μl were applied to the dropped CAMs. Embryos with tumor cell grafts were incubated further in a stationary 37°C humidified incubator. Where indicated, the developing tumors were treated topically on day 1 after tumor cell grafting with 25 μg of control goat IgG or goat anti-VEGF antibody (R&D Systems, Minneapolis, MN; AB-108-C and AB-293-NA, respectively) in 100 μl PBS/5% dimethyl sulfoxide. For the uPA studies, 25 μg function-blocking anti-uPA mAb-112 and mAb-2,[14] or normal mouse IgG (Jackson ImmunoResearch Laboratories, West Grove, PA) were topically applied in 100 μl PBS/5% dimethyl sulfoxide on days 2 and 4 after tumor cell grafting. As a positive control for inhibition of serine proteases, aprotinin was applied at 0.5 trypsin inhibitor units (TIU) per embryo. On

day 7, primary tumors were excised and weighed, and either fixed in 10% Zn-formalin or dissociated for *in vitro* propagation (see below). Portions of the CAM, distal to the primary tumor site (so-called "lower CAM") were harvested and frozen on dry ice for quantitative *Alu*-PCR analysis to determine actual numbers of intravasated tumor cells and, where indicated, dissociated for *in vitro* selection.

In Vivo *Selection of PC-3 Cell Dissemination Variants*

Primary tumors were excised from the CAM under sterile conditions, washed in SF-DMEM, minced and incubated for 3 hours in the presence of 2 mg/ml dispase in SF-DMEM. The dissociated tissue was then passed through 70 μm cell strainers, washed in D-10, and the resultant cell suspensions from individual tumors were pooled and seeded for propagation *in vitro* in D-10. After 2 to 3 weeks, the expanded tumor cells were grafted onto new CAMs for another round of tumor growth and cell isolation. This process of tumor cell grafting followed by tumor cell isolation was repeated seven times, yielding a series of "Tu-1" to "Tu-7" cell lines. The Tu-7 subline was then grafted on the CAM of day 10 chick embryos for tumor development. After 7 days, portions of CAM, distal from the primary tumor site, were harvested under sterile conditions and dissociated by mechanical mincing and dispase treatment. The dissociated cells were plated for *in vitro* propagation, and within 2 to 3 weeks, visible outgrowths of tumor cells were recognizable by their cobblestone-like appearance within a layer of chick embryonic fibroblasts. These colonies of tumor cells were isolated and pooled, generating a high-disseminating subline of PC-3 (PC-hi/diss).

Chick Embryo Experimental Metastasis Assay

Cell suspensions were prepared at a concentration of 1×10^6 cells per ml SF-DMEM and 100 μl of the cell suspensions were injected i.v. into the allantoic vein of embryos developed for 12 days in a humidified 37°C rotary incubator. After cell injections, the embryos were incubated for an additional 5 days in a stationary incubator, at which time portions of the CAM were harvested for *Alu*-qPCR analysis.

Murine Spontaneous Metastasis Models

Six- to 8-week-old male immunodeficient *nu/nu* and SCID mice were purchased from the Scripps Research Institute breeding colony and maintained under the guidelines of the Scripps Research Institute Institutional Animal Care and Use Committee. For implantation under the renal capsule, *nu/nu* mice were anesthetized with a mixture of xylazine and ketamine (12.5 and 100 mg/kg, respectively). An incision was made on the left dorsal region to expose the kidney. 1×10^6 PC-lo/diss cells in a volume of 7 μl or 5×10^5 PC-hi/diss cells in a volume of 4 μl were grafted under the kidney capsule. The kidney was returned to its normal location and incisions were closed with sutures. After 25 days, mice were sacrificed. Tumor weights were determined by subtracting the weight of the contralateral kidney. Liver and lung samples were harvested and frozen for *Alu*-qPCR analysis.

For orthotopic implantation into the prostate, severe combined immunodeficient mice were anesthetized as described above. An incision was made in the lower abdomen to expose the anterior prostate. A total of 2.5×10^6 firefly luciferase labeled PC-hi/diss or PC-lo/diss cells were injected into the prostate in a volume of 25 μl SF-DMEM, and the abdominal incisions were closed with sutures. Live animal imaging was performed after 4 to 5 weeks of tumor growth using the IVIS system (Xenogen Corp, Alameda, CA). Mice were injected i.p. with 3 mg luciferin (*Caliper* Life Sciences, Hopkinton, MA) in 100 μl PBS and imaged in IVIS to monitor primary tumor growth and development of metastases. PC-hi/diss bearing mice were sacrificed between 5 to 6 weeks after tumor cell inoculation when mice became moribund and/or developed ascites. PC-lo/diss bearing mice were sacrificed later, at up to 7 weeks to allow tumors to reach similar size to PC-hi/diss tumors. Images of primary tumors, lymph nodes, and mesenterium were taken with a digital camera. The excised tumors were weighed and fixed in Zn-formalin. Liver, lung, spleen, and lymph node samples were harvested and frozen for *Alu*-qPCR analysis or fixed in Zn-formalin for histological analysis.

Quantitative Alu-PCR Analysis

Quantification of disseminated human tumor cells in chick or murine organs was performed essentially as described.[9,10] Briefly, genomic DNA was extracted from the tissue of interest using the Puregene DNA purification system (Genta Systems, Qiagen, Minneapolis MN). Real time PCR was performed to amplify primate-specific Alu repeat sequences using 10 ng extracted genomic DNA as a template in a Bio-Rad myIQ light cycler. The dsDNA binding dye SYBR green (Molecular Probes, Invitrogen, Carlsbad, CA) was used for quantification. The cycle threshold (Ct) values were converted into numbers of human cells using a standard curve generated by spiking constant numbers of chicken (or murine) cells with serial dilutions of human tumor cells.

In Vitro *Adhesion, Migration, and Invasion*

For haptotactic adhesion experiments, wells of 96 well clusters were pre-coated overnight at 4°C with 5 μg/ml type I collagen, 10 μg/ml fibronectin or 10 μg/ml growth factor reduced Matrigel (BD Biosciences, Franklin Lakes, NJ). PC-lo/diss and PC-hi/diss cells in SF-DMEM were plated on the layers of matrix proteins and allowed to adhere for 45 minutes. Non-adherent cells were washed out and adherent cells were fixed and stained in 0.2% crystal violet solution in 10% ethanol. After washing with PBS, the incorporated dye was extracted with 100 mmol/L sodium phosphate in 50% ethanol (pH 4.5) and optical density measured at 560 nm.

In migration and invasion experiments, 1×10^5 PC-hi/diss or PC-lo/diss cells were plated in 100 μl of SF-DMEM in the upper chamber of 8 μm pore Transwells in 24 well clusters (Corning, Corning, NY). For invasion experiments, the upper side of Transwell membranes was precoated with 2 μg Matrigel to create a matrix barrier. Chemotactic migration and invasion were induced by conditioned medium (CM) from human microvascular endothelial cells (HMVECs) or chick embryonic fibroblasts (CEFs) incubated in serum-free conditions. CM was diluted 1:1 with SF-DMEM and 500 μl were placed in the outer chamber. Where indicated, 25 μg/ml normal mouse IgG or mAb-112, or 0.5 TIU/ml aprotinin were added to both the upper and lower chambers. Haptotactic migration, performed in SF-DMEM, was induced by type I collagen precoated at 2 μg/well on the underside of the Transwell membrane. All migration/invasion experiments were performed for 48 hours at 37°C, after which time non-adherent cells were collected from the outer chamber, combined with adherent cells detached from the underside of the Transwell membrane with trypsin/EDTA, and counted.

Avian and Murine Angiogenesis Models

The CAM angiogenesis assay was performed essentially as described.[15,16] Briefly, type I rat-tail collagen (BD Biosciences) was neutralized and prepared at a final concentration of 2 mg/ml. Cells were incorporated into the collagen mixture at a final concentration of 1×10^6 per ml collagen solution. Where indicated, function-blocking antibodies (50 μg/ml) or aprotinin (0.5 TIU/ml) were incorporated into the collagen mixture. A total of 30 μl of the final collagen mixture were polymerized between two nylon gridded meshes to form an "onplant." Five to 6 onplants were placed onto the CAMs of shell-less day 10 embryos developing ex ovo (4 to 6 embryos per variable). Angiogenic vessels were scored above the upper mesh after 72 to 96 hours and an angiogenic index (number of grids with newly formed blood vessels over the total number of grids scored) was calculated for each onplant. All experiments were performed at least twice.

Angiogenesis assays in mice were performed as described.[15] Briefly, PC-hi/diss or PC-lo/diss tumor cells were incorporated into 2.5 mg/ml type I collagen from rat tail (BD Biosciences) at a final concentration of 1×10^6 cells per ml. Approximately 50 μl of cell-containing or cell-free collagen mixtures were polymerized at 37°C within hollow silicon tubes (approximately 1.0 cm in length), making an "angiotube." Angiotubes were then inserted into air pockets created by skin incisions on both dorsal sides of anesthetized *nu/nu* mice. Each mouse received a total of four angiotubes (two per flank), and incisions were closed with surgical clamps. Three weeks later, the mice were sacrificed and the skin flap with angiotubes was exposed and photographed. After careful excision, the contents of angiotubes were flushed out and lysed in modified radio immunoprecipitation assay (mRIPA) buffer. Hemoglobin concentration in the lysates was determined using the QuantiChrom Hemoglobin Assay Kit (BioAssay Systems, Hayward, CA), according to the manufacturer's instructions.

Antibody Array and Enzyme-Linked Immunosorbent Analysis

Serum-free conditioned media were collected from PC-hi/diss or PC-lo/diss cell monolayers after 48 hours of incubation. Loading was normalized to cell number per culture at the time of CM collection. TranSignal Angiogenesis Antibody Arrays (Panomics, Fremont, CA) were performed according to the manufacturer's instructions. Densitometry of the positive spots was quantified using an AlphaImager (AlphaInnotech, San Leandro, CA). All values were normalized to the intensity of positive control spots on each membrane. The levels of VEGF in PC-hi/diss and PC-lo/diss CM were analyzed by capture enzyme-linked immunosorbent assay (ELISA) (Peprotech, Rocky Hill, NJ) using the human VEGF ELISA development kit, according to the manufacturer's instructions. VEGF concentrations were quantified using a standard curve of recombinant VEGF protein within the ELISA plate.

Immunohistochemistry

Primary tumors and murine lungs were excised and fixed in Zn-10% formalin and paraffin-embedded. Deparaffinized tissue sections were treated with 0.3% hydrogen peroxide and blocked with PBS supplemented with 2% bovine serum albumin and 5% normal goat serum. For detection of human cells, tissue sections were treated with antigen unmasking solution (Vector Laboratories, Burlingame, CA) and stained with 1 μg/ml mAb 29-7, which specifically recognizes human, but not chicken or murine, CD44. After washing, the slides were incubated for 1 hour with secondary biotinylated goat anti-mouse IgG (1:1000). For vascular staining, CAM tumor sections were treated with Pepsin DAKO for 10 minutes at 37°C, followed by staining for 1 hour with 1 μg/ml Biotinylated Elderberry Bark Lectin (Sambucus *nigra* agglutinin, SNA), purchased from Vector Labs. The 29-7 or SNA stained sections were then incubated with Avidin-D horseradish peroxidase conjugate (Vector Laboratories) for 30 minutes and developed with a diaminoenzidine chromogenic substrate. Sections were counterstained with Mayer's hematoxylin. Images were captured using an Olympus BX60 microscope equipped with a digital DVC video camera and processed with Adobe Photoshop 6.0 software. For vessel quantification, serial images were taken at $\times$20 original magnification and the number of lumen-containing vessels per arbitrary grid of tumor-filled tissue was determined in 10 to 20 individual images per tumor section with a total of 3 to 5 different tumors analyzed per variable.

Western Blot Analysis

PC-hi/diss and PC-lo/diss cells were lysed in mRIPA buffer containing protease inhibitors (aprotinin, leupeptin, and pepstatin, each at 10 μg/ml, and phenylmethylsulfonyl fluoride at 1 mmol/L) for 30 minutes at 4°C. Cell lysates were clarified by centrifugation and protein concentration was determined by BCA assay (Pierce). For secreted proteins, 90% confluent cell monolayers were

incubated with or without 25 μg/ml mAb-112 or 0.1 TIU/ml aprotinin in SF-DMEM. After 48 hours, CM was collected, and adherent cells detached with trypsin/EDTA and counted to normalize loading of CM. To verify that loaded samples of PC-hi/diss and PC-lo/diss CM contained similar protein levels, CM was concentrated tenfold and resolved by 4% to 20% SDS-polyacrylamide gel electrophoresis (PAGE). Similar intensity of the major protein bands was confirmed following staining of the gel with Coomassie blue (data not shown). Equal amounts of proteins from cell lysates or normalized volumes of CM were resolved on 4% to 20% SDS-PAGE and transferred to Immobilon-P PVDF membranes (Millipore, Billerca, MA). After transfer, the membranes were blocked with 5% nonfat milk in PBS plus 0.05% Tween 20. Membranes were probed overnight at 4°C with the following primary antibodies: murine anti-E-Cadherin (BD), murine anti-N-Cadherin (BD Bioscienses), murine anti-Vimentin (Neomarkers, Fremont, CA), goat anti-uPA recognizing single-chain zymogen and B chain (American Diagnostica, Stamford, CT, #398), or rabbit anti-uPA recognizing single chain zymogen and A and B chains of activated enzyme.[14] Membranes were washed in PBS plus 0.05% Tween 20 and probed with horseradish peroxidase conjugated secondary antibodies (anti-mouse horseradish peroxidase from Bio-Rad, Hercules, CA; or anti-rabbit horseradish peroxidase from GE Health care, Piscataway, NJ). After washes in PBS plus 0.05% Tween 20, immunoreactive bands were visualized using SuperSignal West Pico Chemiluminescent Substrate (Pierce, Rockford, IL) and quantified with a Molecular Imager Gel Doc XR System (Bio-Rad).

Data Analysis and Statistics

Data processing and statistical analysis were performed using GraphPad Prism Software (GraphPad Software, Inc., San Diego, CA). Numbers of samples analyzed and experiments performed are indicated in the Figure Legends. Data are presented as means ± SEM from a representative experiment or several normalized experiments, where percent changes were calculated from the pooled fold differences determined by taking ratios of numerical values for individual embryos over the mean of the control group. Mann-Whitney test or Student's *t*-test were used to determine significance ($P < 0.05$) of differences between data sets.

Results

Selection of PC-3 Cell Dissemination Variants Using the Chick Embryo Model

In the chick embryo spontaneous metastasis model, 2.0×10^6 parental PC-3 cells generated 100 to 200 mg primary tumors within 7 days after grafting on the CAM. However, PC-3 cells lack the capacity to spontaneously intravasate into the CAM vasculature and disseminate to the distal CAM or internal organs. An *in vivo* selection strategy was therefore used to isolate from the PC-3 parental line a cell variant capable of efficient spontaneous metastasis. Briefly, our strategy involved serial *in vivo* passages of PC-3 cells isolated from primary CAM tumors (Figure 1A). Primary tumor weights tended to increase with each round of tumor-to-tumor passaging (Figure 1B, top). After two rounds of *in vivo* passaging of PC-3 cells, intravasated cells were detected by *Alu*-qPCR, albeit at low levels and with low incidence among host embryos, suggesting that cells with intravasation potential were present within the primary tumor. A total of seven tumor-to-tumor passages were performed, yielding gradually increasing numbers of disseminated PC-3 cells in the distal CAMs (Figure 1B, bottom, "Tu1-Tu7"). Finally, intravasated tumor cells were isolated from the distal, or lower, CAM (LC) of embryos that received "PC-Tu7" cells and were expanded *in vitro* and pooled, generating the "PC-LC" cell line. When reapplied to the CAMs of chick embryos, PC-LC cells formed sizable (200 to 300 mg) primary tumors and efficiently intravasated into the CAM vasculature (Figure 1B, "LC"). Importantly, PC-LC cells were detected in distal CAMs at further elevated concentrations compared with all PC-Tu variants, yielding 1000 to 5000 intravasated cells per 10^6 host cells. Thus, the PC-LC subline represents a highly disseminating variant of the parental PC-3 cell line and will be referred to as PC-hi/diss. A subline of PC-3 cells, isolated after one round of *in vivo* CAM tumor growth ("PC-Tu1"), was used in comparative studies as a PC-hi/diss counterpart since it had been exposed to the *in vivo* microenvironment, resulting in improved tumor growth, but retained extremely low-disseminating ability (Figure 1B, "Tu-1"). This low disseminating PC-3 cell variant will be referred to as PC-lo/diss.

The PC-lo/diss and PC-hi/diss cells formed histologically similar primary tumors that differed by approximately twofold in weight (Figure 1B, top). However, the difference in intravasation was much more profound, with PC-hi/diss yielding on average 40-fold higher levels of intravasation over PC-lo/diss (Figure 1B, bottom). Since the PC-hi/diss variant forms larger primary tumors, it could be argued that the observed increase in intravasation was due to the increased tumor mass. To address this possibility, the intravasation levels were compared retrospectively between embryos bearing PC-lo/diss and PC-hi/diss tumors of similar weight (ranging from 160 to 200 mg). This analysis demonstrated that even when primary tumors reached similar sizes, intravasation dramatically and significantly differed by approximately 100-fold (Figure 1C). Additionally, proliferation rates *in vitro* were compared between the PC-3 cell variants and found to be nearly identical, ruling out any profound difference in growth characteristics (see Supplemental Figure S1A at *http://ajp.amjpathol.org*).

To verify that the differential in dissemination capacity was due to early events leading to intravasation as opposed to late events in metastasis such as extravasation and colonization, the PC-3 variants were compared in an experimental metastasis assay. In this assay, cells were directly injected into the allantoic vein of developing chick embryos. PC-hi/diss and PC-lo/diss cells differed by less than twofold in their ability to colonize the CAM in this assay (Supple-

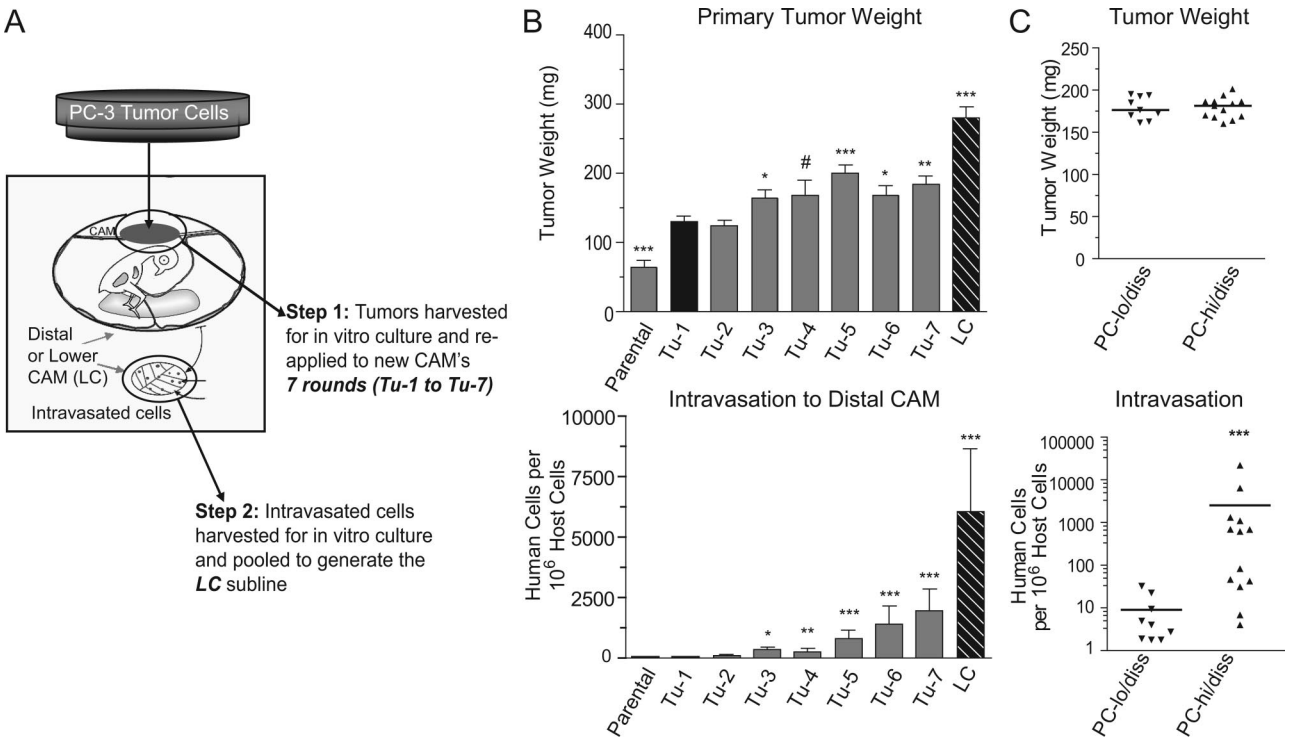

Figure 1. In vivo selection of PC-3 dissemination variants and their characterization in the chick embryo spontaneous metastasis model. **A:** Schematic presentation of multiround selection of dissemination variants from the prostate carcinoma PC-3 cell line. Following grafting on the CAM, the developed tumors were harvested, expanded *in vitro* and re-applied to new CAMs. A total of 7 rounds of *in vitro-in vivo* passaging were performed, yielding a series of primary tumor-derived cell lines (Tu-1 to Tu-7). After the seventh round, intravasated cells were isolated from the distal CAM ("Lower CAM"), yielding the LC cell line. **B:** Isolated PC-3 cell lines were analyzed for their efficiency in tumor growth (**top**) and intravasation (**bottom**) in the chick embryo spontaneous metastasis model. Data are means ± SEM from 1 to 5 independent experiments performed with each cell variant. **C:** A retrospective analysis of tumor cell intravasation (**bottom**) in individual embryos bearing PC-lo/diss and PC-hi/diss primary tumors of similar size, 160 to 200 mg (**top**). Statistical significance of the differences was analyzed in comparison with Tu-1 cell line: $^{\#}P < 0.05$, one-tailed *t*-test; $^{*}P < 0.05$, $^{**}P < 0.01$; and $^{***}P < 0.0001$ in two-tailed *t*-test (**B**, **top**) or Mann-Whitney test (**B, bottom**; **C**).

mental Figure S1B at *http://ajp.amjpathol.org*). Therefore, the 40- to 100-fold dissemination differential between the PC-3 variants appears to lie primarily in their capacity to successfully complete early steps of the metastatic cascade, culminating in intravasation into the CAM vasculature.

High Metastatic Potential of PC-hi/diss in Spontaneous Metastasis Models in Mice

To confirm that the increased dissemination potential of the selected PC-hi/diss variant was not attributed to a specific adaptation to the avian microenvironment used for selection, spontaneous metastasis of the PC-3 cell variants was also evaluated in two murine model systems, ie, a renal capsule model, exploiting the rich vascular microenvironment of the kidney, and a prostate orthotopic model.

In the renal capsule model, the PC-hi/diss and PC-lo/diss tumor cells were inoculated under the kidney capsule of immunodeficient mice, where they formed primary tumors of similar size (300 to 600 mg) within 20 to 25 days after transplantation (Figure 2, A and B). However, PC-hi/diss yielded higher levels of spontaneous metastasis compared with PC-lo/diss as detected by *Alu*-qPCR. There was a substantial 13.6-fold differential in liver metastasis (Figure 2C) and a clear twofold differential in metastases to the lungs between the animals bearing PC-hi/diss versus PC-lo/diss tumors (data not shown). Thus, the increased dissemination ability of PC-hi/diss, initially observed in the chick system, was affirmed in this mammalian spontaneous metastasis model.

To determine whether PC-hi/diss would be also differentially aggressive in an orthotopic spontaneous metastasis model, PC-hi/diss and PC-lo/diss cells were pre-labeled with firefly luciferase (fluc) to allow for non-invasive live animal imaging, and surgically implanted into the anterior prostates of SCID mice. Both cell variants formed primary tumors within the prostates in 4 to 6 weeks, as first indicated by bioluminescence in the prostate region (Figure 3A). The levels of bioluminescence in animals bearing PC-hi/diss tumors were slightly higher than in the mice with developing PC-lo/diss tumors. In addition, only mice with PC-hi/diss tumors demonstrated high levels of bioluminescence in the abdomen, in the liver and in the spleen areas (Figure 3B). The presence of expanding primary tumors in the prostates was confirmed on dissection of sacrificed animals, demonstrating similar gross morphology of the tumors (Figure 3C), although the PC-lo/diss cells generally gave rise to smaller tumors (Figure 3D). The localization of human tumor cells within characteristic prostate glandular tissue was indicated by histological analysis after H&E staining (Figure 3E, left panel) and confirmed by immunohistochemical analysis after staining of primary tumors for human CD44 (Figure 3E, middle panel). Both cell lines efficiently metastasized to axillary

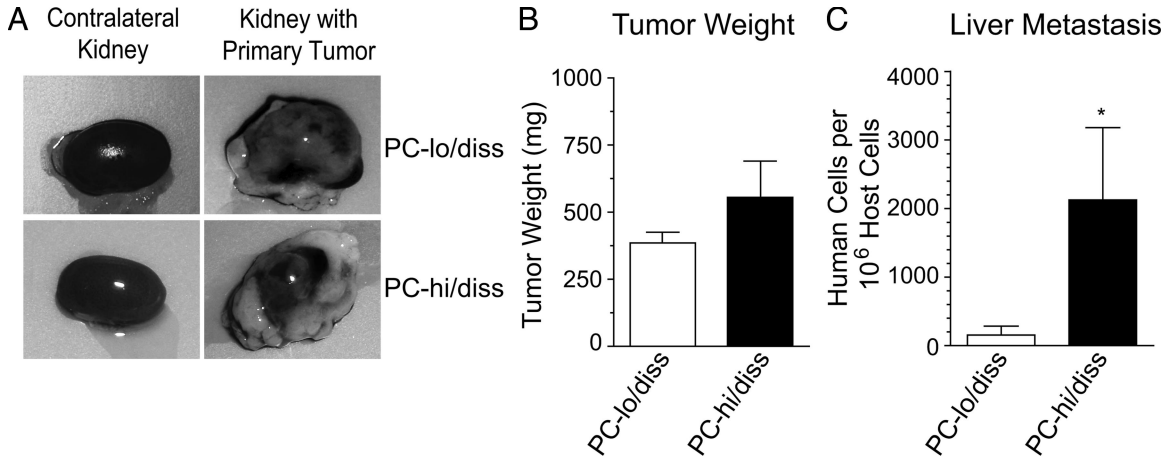

Figure 2. Dissemination of PC-3 variants in the renal capsule spontaneous metastasis model. **A:** Selected PC-lo/diss and PC-hi/diss cells were grafted under the kidney capsule of *nu/nu* mice. Large primary tumors developed on the kidneys and almost completely engulfed them within 4 to 5 weeks post implantation (**right panels**). For comparison, contralateral kidneys are shown on the left. **B:** The net weight of individual primary PC-lo/diss and PC-hi/diss tumors was estimated by subtracting the weight of the contralateral kidney. Data are means ± SEM from a representative experiment using 4 mice per variant. **C:** Metastasis levels in the livers of mice bearing PC-lo/diss (open bars) and PC-hi/diss (closed bars), quantified by *Alu*-qPCR. $^*P < 0.05$ in one-tailed Mann-Whitney test.

and inguinal lymph nodes, as indicated by lymph node enlargement (Figure 3C). However, dissemination of cells from primary PC-hi/diss tumors to the lymph nodes appears to be sixfold more efficient than from their low disseminating counterpart (Figure 3F). In addition, widespread abdominal metastases developed in all (6 out of 6) PC-hi/diss tumor-bearing animals, manifested by ascites and numerous large tumor nodules within the mes-

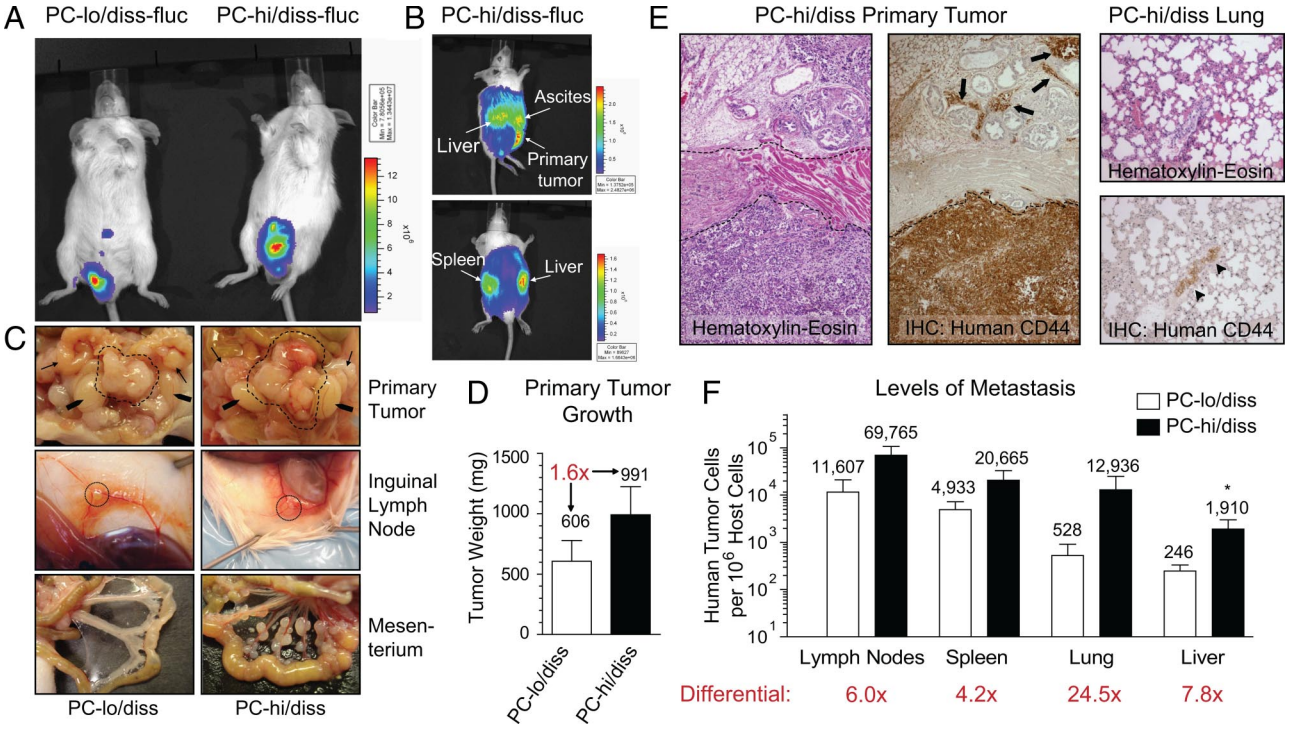

Figure 3. Characterization of PC-3 dissemination variants in an orthotopic spontaneous metastasis model. **A:** Bioluminescence imaging of PC-lo/diss or PC-hi/diss primary tumors in SCID mice 5 weeks after surgical implantation of firefly luciferase-tagged cells (fluc) into anterior prostates. **B:** Bioluminescence imaging from side (**top**) and dorsal (**bottom**) views of a mouse bearing a PC-hi/diss tumor 5 weeks after implantation. High levels of bioluminescence are associated with the primary tumor, liver, spleen, and abdominal ascites. **C:** Gross morphology of primary tumors, lymph nodes and mesenterium in sacrificed mice. The tumors in the prostate area are circumscribed by dotted lines (**top panels**). **Arrows** point to seminal vesicles, **arrowheads** point to testes. Significantly enlarged inguinal (subiliac) lymph nodes are indicated by circles (**middle panels**). The mesenterium in PC-hi/diss-bearing mice is heavily inseminated with macroscopic metastatic nodules (**bottom panels**). **D:** Primary tumors were excised and weighed, indicating a 1.6-fold difference in tumor size between the two PC-3 variants. **E:** H&E staining of a PC-hi/diss tumor (**left panel**) indicates the presence of a tumor cell mass at the bottom of the section and tumor invasion between prostate glands at the **top** of the section. A muscular layer in the **middle** is indicated by dotted lines. The presence of human tumor cells invaded the prostate glandular tissue (**arrows**) was confirmed by immunohistochemical staining with mAb 29-7, specifically recognizing human CD44 (**middle panel**). A section of lung tissue from a mouse bearing PC-hi/diss tumor (**right panels**) stained with H&E (**top**). Immunohistochemical staining for human CD44 (brown) confirms the presence of metastatic lesion indicated by the **arrowhead** (**bottom**). **F:** Levels of metastasis in mice bearing PC-lo/diss (open bars) and PC-hi/diss (closed bars) tumors were determined by *Alu*-qPCR in the lymph nodes, spleen, lung, and liver. Bars are means ± SEM from two independent experiments using six mice total per variant. Numbers above bars are mean numbers of humans cells quantified in the organ per 10^6 murine cells. $^*P < 0.05$ in one-tailed Mann-Whitney test.

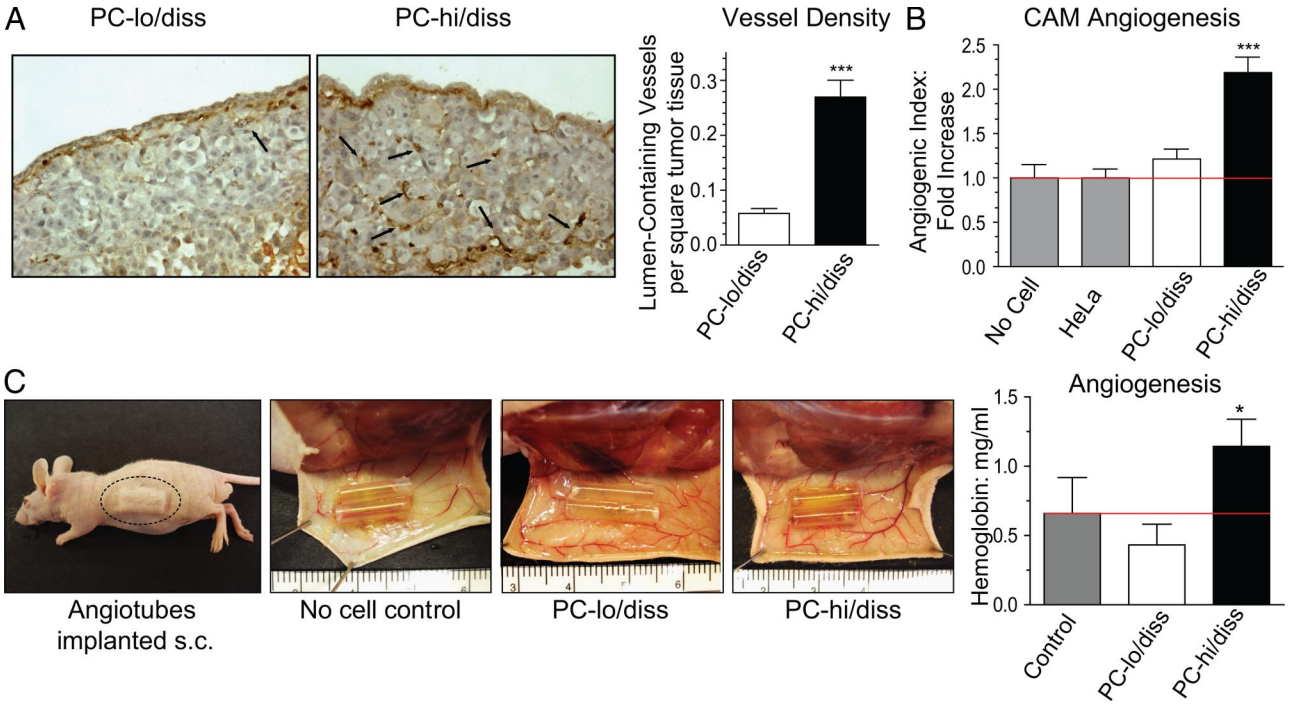

Figure 4. Angiogenic potential of PC-3 intravasation variants in chick embryo and mouse models. **A:** Tumor angiogenesis in the CAM spontaneous metastasis model. PC-lo/diss and PC-hi/diss primary CAM tumors were stained with SNA lectin to highlight endothelial cells (**left panels**). **Black arrows** point to lumen-containing blood vessels. Vessel density was determined as a ratio of arbitrary grids with lumen-containing vessels per total number of grids analyzed in digital images of tissue sections taken at ×20 original magnification. From 10 to 20 images per tumor in 3 to 5 individual tumors per variable were analyzed to calculate the means ± SEM presented in the bar graph. **B:** Angiogenic potential of PC-3 variants in the CAM collagen onplant model. PC-lo/diss and PC-hi/diss cells were incorporated into collagen onplants grafted on the CAM of shell-less chick embryos. The onplants containing collagen alone or non-angiogenic HeLa cells were used as negative controls. The angiogenic index was calculated at 72 hours as the number of grids containing vessels over total number of grids scored in four independent experiments (number of onplants, $n = 14$, no cells; $n = 63$, HeLa; $n = 45$, PC-lo/diss; $n = 79$, PC-hi/diss). The data are presented as fold difference compared with the angiogenic index of collagen onplants containing HeLa cells. $^{***}P < 0.0001$ in two-tailed Student's *t*-test. **C:** Angiogenic potential of PC-3 variants in the mouse angiotube model. Silicon tubes (angiotubes) containing collagen alone (no cell control) or PC-hi/diss or PC-lo/diss tumor cells were implanted under the skin of *nu/nu* mice (**left panel**). At 3 weeks, the mice were sacrificed, and the skin flaps with the angiotubes exposed, indicating visually more blood vessels around the PC-hi/diss containing tubes than either control (collagen alone) or PC-lo/diss containing tubes (**middle panels**). Levels of angiogenesis were estimated by measuring hemoglobin concentration in the contents of individual angiotubes ($n = 8$ per variable) (bar graph). Bars represent means ± SEM from a representative experiment. $^{*}P < 0.05$ in two-tailed Student's *t*-test.

enterium (Figure 3C, lower panels). Only 2 of 6 PC-lo/diss mice presented with ascites and/or tumor cell colonization of the mesenterium, although the PC-lo/diss bearing mice were allowed an additional week of tumor development. Importantly, PC-hi/diss tumors were significantly more metastatic to the liver (eightfold; $P < 0.05$) and were clearly more efficient in their spread to the lung (24.5-fold; $P = 0.066$) and spleen (fourfold; $P = 0.12$) as determined by *Alu*-qPCR analysis in comparison with PC-lo/diss tumors (Figure 3F). In PC-hi/diss bearing animals, microscopic foci of tumor cells were also identified within the lung parenchyma by immunohistochemical staining for human CD44 (Figure 3E, right panels). Thus, in this orthotopic model, as in the mouse kidney capsule and chick embryo spontaneous metastasis models, PC-hi/diss cells were clearly more aggressive; these *in vivo* selected cells formed larger and rapidly growing primary tumors and metastasized more efficiently than the PC-lo/diss counterparts.

Contribution of Tumor Angiogenesis to PC-hi/diss Intravasation

Tumor angiogenesis is often correlated with tumor progression and high-grade (ie, metastatic) disease, and the possibility of a link between angiogenesis and metastasis prompted us to determine whether the PC-3 cell variants might differentially induce angiogenesis and whether a difference in angiogenic potential might have a functional impact on their dissemination capabilities. To this end, levels of angiogenesis were compared between primary PC-hi/diss and PC-lo/diss CAM tumors. Sections of CAM tumors were stained with SNA lectin to highlight the endothelial cells and allow visualization of the tumor vasculature (Figure 4A). Scoring of intratumoral vessel density in serial images indicated that PC-hi/diss primary CAM tumors contained substantially more (4.6-fold, $P < 0.0001$) lumen-containing vessels per arbitrary square filled with tumor tissue (Figure 4A, bar graph).

In addition, the ability of the two cell variants to induce angiogenesis in a quantitative and easily manipulatable CAM angiogenesis model[15] was investigated. In this model, collagen droplets impregnated with tumor cells were allowed to polymerize on nylon grids before grafting on the CAM of day 10 shell-less embryos developing ex ovo; 72 to 96 hours later these 'onplants' were scored for new vessel development. When PC-hi/diss and PC-lo/diss cells were incorporated into collagen onplants, only PC-hi/diss efficiently induced angiogenesis over control levels observed in onplants containing collagen alone or

impregnated with HeLa cells characterized by low angiogenic potential (Figure 4B).

The differential in angiogenic potentials of the PC-3 variants was further confirmed using a murine model, where silicon tubes filled with collagen alone or a mixture of collagen and tumor cells (angiotubes) were implanted under the skin of immunodeficient mice (Figure 4C, left panel). Three weeks after implantation, the growth of blood vessels was visually compared between angiotubes containing PC-hi/diss versus PC-lo/diss cells or collagen alone. As can be seen in Figure 4C, blood vessels appeared to be converging at the openings of the cell-containing angiotubes. Importantly, PC-hi/diss induced the formation of a more robust blood vessel network around the angiotubes compared with the no cell control and the PC-lo/diss variant. Hemoglobin content within the tubes was measured as an indicator of angiogenesis. Confirming our observations in the chick model systems, only the PC-hi/diss variant was highly angiogenic in contrast to the PC-lo/diss cells, which did not induce angiogenesis over control levels (Figure 4C, bar graph). Thus three distinct angiogenesis assays in two separate animal models demonstrated a significant differential in the ability of PC-hi/diss and PC-lo/diss to induce angiogenesis.

To analyze potential differences in secretion of individual angiogenic factors that might underlie the differential in angiogenic phenotype of the PC-3 intravasation variants, we used an antibody array in which levels of secreted angiogenic factors were compared in the conditioned media (CM) of PC-lo/diss and PC-hi/diss. This array highlighted a twofold differential in VEGF production by the PC-3 dissemination variants (Figure 5A). The differential in the levels of secreted VEGF was further confirmed and quantified by capture ELISA (Figure 5B). To address whether high levels of PC-hi/diss-induced angiogenesis could be attributed to the increased VEGF secretion, we used a function-blocking anti-VEGF antibody, which was incorporated into PC-hi/diss-containing collagen onplants. This antibody significantly decreased PC-hi/diss induced angiogenesis to the levels observed for PC-lo/diss (Figure 5C), thus supporting our suggestion that the high levels of angiogenesis induced by PC-hi/diss were dependent on the elevated VEGF levels.

To analyze whether this VEGF-dependent increase in tumor angiogenesis was functionally important for PC-hi/diss dissemination, we diminished the levels of VEGF in PC-hi/diss tumors by treating the developing CAM tumors with the function-blocking antibody to human VEGF, and monitored vessel density, tumor growth, and spontaneous metastasis. Four days after tumor cell grafting, a subset of primary tumors was fixed and stained for human CD44 to highlight human tumor cells and the tumor-CAM border and also with SNA to highlight host endothelial cells (Figure 5D). Serial microscopic images were analyzed to determine the vessel density within the primary tumors. This analysis indicated a significant 30% reduction in vessel density in tumors treated with anti-VEGF (Figure 5E), suggesting efficacy of the strategy to reduce tumor angiogenesis. After seven days of tumor growth on the CAM, primary tumors were excised,

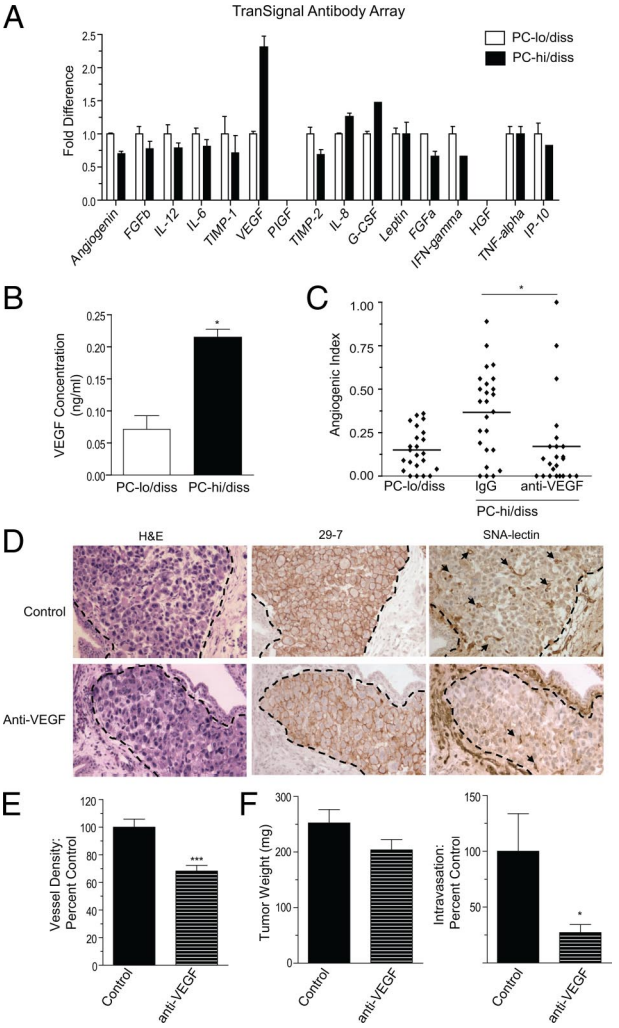

Figure 5. Increased VEGF production contributes to enhanced angiogenesis and intravasation of PC-hi/diss. **A:** Analysis of pro- and anti-angiogenic factors produced by PC-lo/diss and PC-hi/diss cells. Serum-free CM from PC-lo/diss and PC-hi/diss cell monolayers was assayed by a TranSignal Angiogenesis Antibody Array, indicating differential in secreted VEGF. **B:** Levels of VEGF in the CM of PC-hi/diss and PC-lo/diss were quantified by a capture ELISA. **C:** Contribution of VEGF to PC-hi/diss-induced angiogenesis in the CAM collagen onplant model. A function-blocking antibody to VEGF (R&D) was incorporated at 50 μg/ml into collagen onplants containing PC-hi/diss cells (3×10^4 cells per onplant). Angiogenic index was determined at 72 hours in comparison with onplants containing PC-lo/diss cells. In the scattergram, lines represent means from angiogenic indices determined for each individual onplant in a representative experiment using 5 to 6 embryos per variant (23 to 25 onplants). **D:** Contribution of VEGF to PC-hi/diss-induced angiogenesis in the chick embryo spontaneous metastasis model. Primary PC-hi/diss CAM tumors were treated topically with the control IgG or function-blocking antibody to VEGF. After 4 days, 3 to 5 control or anti-VEGF-treated tumors were harvested, fixed, and stained with H&E, immunostained with mAb-29-7 against human CD44 to identify tumor cells (brown cell membrane staining), or stained with SNA to highlight the vasculature. Dotted lines delineate the tumor borders. **Arrows** point to lumen-containing blood vessels. **E:** Vessel density was calculated after scoring lumen-containing blood vessels in control and anti-VEGF-treated PC-hi/diss tumors in a series of SNA stained tumor sections. Images and vessel density analysis are from a representative experiment, in which three tumors were analyzed per variable with 10 to 20 images analyzed per tumor. **F:** Contribution of VEGF to PC-hi/diss intravasation in the spontaneous metastasis CAM model. At day 7, control IgG and anti-VEGF-treated PC-hi/diss tumors were harvested and weighed (**left panel**), and intravasated tumor cells in the distal CAM were quantified by *Alu*-qPCR (**right panel**). Tumor weights and intravasation data are pooled values from three individual metastasis experiments with total of 25 and 22 embryos treated with control IgG and anti-VEGF, respectively. $^{\#}P < 0.05$ in one-tailed Mann Whitney test; $^{*}P < 0.05$, $^{**}P < 0.01$, and $^{***}P < 0.0001$ in two-tailed Student's *t*-test.

weighed and dissemination of tumor cells to the distal CAM was quantified by *Alu*-qPCR. While the anti-VEGF treatment had only a marginal effect on tumor growth (Figure 5F, left bar graph), dissemination to the distal CAM was substantially decreased to 27% of control levels (Figure 5F, right bar graph). Taken together, these data suggest that targeting VEGF not only reduces tumor-induced angiogenesis and microvessel density within developing CAM tumors, but also concomitantly reduces PC-hi/diss cell intravasation and dissemination within the CAM vascular network.

Adhesion, Migration and Invasion of PC-3 Dissemination Variants

Intravasation of tumor cells into intratumoral angiogenic vasculature or peritumoral pre-existing blood vessels would require implementation of escape mechanisms by aggressive tumor cells, including dissociation from the primary tumor, invasion of surrounding tissue and migration toward blood vessels. To address potential differences in escape mechanisms between PC-lo/diss and PC-hi/diss, we subjected the cell variants to a series of *in vitro* assays to compare their adhesion, migration and invasion characteristics. The PC-hi/diss cells were less adhesive to the purified extracellular matrix proteins collagen I and fibronectin and to the basement membrane proteins of Matrigel (Figure 6A). Since endothelial cells and fibroblasts would be the two major cell types encountered by escaping tumor cells within the tumor microenvironment, we analyzed the respective abilities of PC-hi/diss and PC-lo/diss to migrate chemotactically toward conditioned media from these two cell types. PC-hi/diss cells displayed increased ability to chemotactically migrate toward CM from HMVECs and CEFs in Boyden-type chamber assays (Figure 6B). Additionally, PC-hi/diss cells were significantly more migratory in haptotactic migration induced by type I collagen in the absence of additional chemotactic stimuli (Figure 6C). When Transwells were coated with Matrigel to create an extracellular matrix barrier, the PC-hi/diss cells manifested increased ability to invade through Matrigel toward chemotactic stimuli present in fibroblast CM (Figure 6D).

The enhanced migratory and invasive characteristics observed in PC-hi/diss were suggestive of a partial epithelial to mesenchymal transition (EMT), a process that has been well described in embryonic development and recently linked to carcinoma progression,[17,18] as carcinoma cells lose some of their epithelial characteristics and gain a more migratory, mesenchymal phenotype. The possibility that PC-hi/diss cells had undergone EMT was addressed by Western blot and qPCR analysis of classical EMT markers. There was a substantial reduction in levels of the epithelial marker E-cadherin at both the protein (11-fold) and message (22-fold) levels in PC-hi/diss compared with PC-lo/diss. Levels of the mesenchymal marker N-cadherin, however, were similar between the two variants, and vimentin, a second mesenchymal marker, was not detected in either of the two PC-3 cell

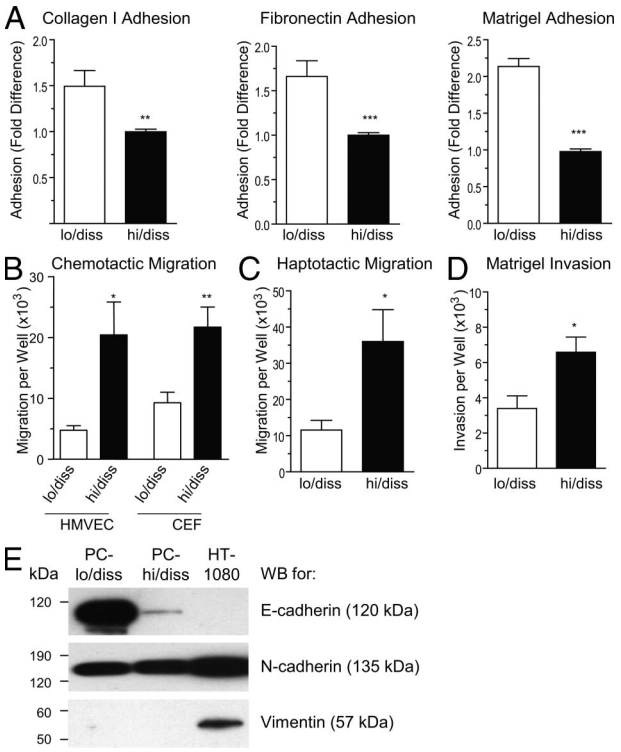

Figure 6. *In vitro* characteristics of PC-lo/diss and PC-hi/diss cell variants. **A:** Adhesion of PC-lo/diss and PC-hi/diss cells to type I collagen, fibronectin, or Matrigel. Data are presented as fold differences of PC-lo/diss adhesion in comparison with adhesion levels of PC-hi/diss, determined from 3 independent experiments performed in triplicate. **B:** Chemotactic migration of PC-lo/diss and PC-hi/diss cells in Transwells was induced by serum-free CM from CEFs or HMVECs placed into the outer chamber. **C:** Haptotactic migration of PC-lo/diss and PC-hi/diss cells in Transwells was stimulated by type I collagen coated onto undersurface of the membrane. **D:** Matrigel invasion of PC-lo/diss and PC-hi/diss cells induced by CM from CEFs placed into the outer chamber. Data are presented as means ± SEM of cells recovered from individual outer chambers following a 48 hour migration or invasion in three independent experiments performed in duplicate. $^{*}P < 0.05$, $^{**}P < 0.01$, and $^{***}P < 0.001$ in two-tailed Student's *t*-test. **E:** Western blot analysis of PC-lo/diss, PC-hi/diss and HT-1080 cell lysates (20 to 50 μg/lane) for E-cadherin, N-cadherin, and vimentin. Position of molecular weight markers is indicated in kDa on the left.

variants in contrast to high levels of this protein expressed in the mesenchymal tumor cell line HT-1080 used as a positive control (Figure 6E). Finally, mRNA levels of three EMT-inducing transcription factors (ie, Slug, Snail and Twist)[19,20] were similar between the two cell variants, as determined by quantitative PCR (data not shown). Together, these data suggest that although the PC-hi/diss cells display some characteristics of cells that have undergone EMT (ie, substantial loss of E-cadherin, decreased adhesion and increased migration and invasion), the overall molecular changes normally accompanying carcinoma EMT were not observed.

Contribution of uPA to PC-hi/diss Invasion and Dissemination

Increases in levels and activity of proteolytic enzymes have been linked to enhanced motility and invasion in tumor cells,[21–23] and specifically the serine protease uPA is often elevated in aggressive carcinomas.[24] Using a

chemical proteomic approach, our lab has previously identified uPA activation as a key step in HT-hi/diss fibrosarcoma cell intravasation[11,14] and we therefore asked the question of whether uPA might contribute to the enhanced invasion and intravasation capacity of PC-hi/diss as well. To this end, we compared levels of single chain uPA proenzyme and the two chain uPA active enzyme in samples of serum-free medium conditioned by equal numbers of adherent PC-hi/diss or PC-lo/diss cells. By Western blot analysis, levels of the 50 kDa species of pro-uPA in the CM of PC-hi/diss were substantially higher (sixfold) than in PC-lo/diss CM (Figure 7A). A threefold differential in active uPA was also indicated by quantifying levels of the 33 kDa B chain in the CM of PC-hi/diss separated by SDS-PAGE under reducing conditions (Figure 7A). To analyze the contribution of the uPA differential to the high-disseminating phenotype of PC-hi/diss, we used function-blocking antibody mAb-112, which specifically blocks uPA zymogen activation by preventing cleavage to the two chain active enzyme[14] and aprotinin, a potent inhibitor of serine proteases including plasmin. When PC-hi/diss cell monolayers were incubated with either mAb-112 or aprotinin, no accumulation of two chain active uPA in the condition media was observed, confirming that both reagents prevented uPA activation *in vitro* (Figure 7B).

To analyze the functional contribution of uPA in facilitating PC-hi/diss intravasation *in vivo*, we used two function blocking monoclonal antibodies: mAb-112 to prevent zymogen *activation*, and mAb-2 to prevent proteolytic *activity* of the enzyme.[14] Aprotinin was also included as a positive control for inhibition of plasmin-mediated activation of uPA. Developing PC-hi/diss CAM tumors were treated topically with anti-uPA antibodies or aprotinin and tumor growth and intravasation were analyzed after 7 days. Each of the antibody treatments slightly decreased primary tumor growth, while aprotinin did not have any effect on tumor weight (Figure 7C, left bar graph). However, the function-blocking antibodies, mAb-112 and mAb-2, both significantly decreased intravasation to the distal CAM to 43% and 47% of control levels, respectively, while aprotinin treatment substantially inhibited intravasation by 90% (Figure 7C), strongly implicating uPA activation and activity in PC-hi/diss dissemination. Interestingly, treatment with mAb-112, mAb-2, or aprotinin did not significantly affect CAM colonization when tumor cells were injected i.v. in the avian experimental metastasis model (data not shown), further highlighting the importance of activated uPA in facilitating those early events in PC-hi/diss dissemination that lead to tumor cell intravasation.

To explore potential mechanisms by which uPA contributes to PC-hi/diss dissemination, we analyzed the role of uPA activation in PC-hi/diss invasion. To this end, mAb-112 or aprotinin were incorporated into *in vitro* Matrigel invasion assays and both effectively reduced PC-hi/diss invasion, by 40% and 67%, respectively (Figure 7D). Thus, active uPA seems to be required for PC-hi/diss cells to proteolytically degrade the basement membrane proteins of Matrigel and invade through a matrix barrier.

In addition to facilitating invasion, serine proteases have been implicated in tumor angiogenesis.[25,26] Since

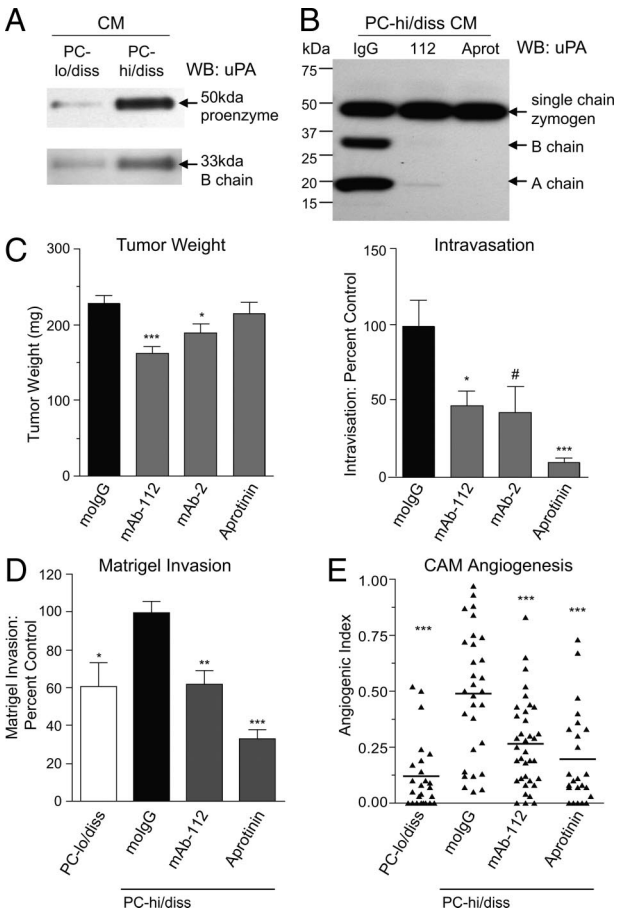

Figure 7. Functional contribution of uPA to PC-hi/diss intravasation, invasion, and angiogenesis. **A:** Western blot analysis of uPA production by PC-lo/diss and PC-hi/diss cell variants. SDS-PAGE of CM, normalized to equal numbers of adherent cells, was performed under reducing conditions allowing for detection of single chain pro-uPA (**top panel**) and B chain of the activated uPA enzyme (**bottom panel**) by goat anti-uPA antibody. **B:** Western blot analysis of uPA activation by PC-hi/diss cells. CM was harvested from PC-hi/diss cell monolayers incubated for 48 hours with control IgG, mAb-112, or aprotinin. SDS-PAGE of CM samples was performed under reducing conditions. Single chain uPA zymogen, and B chain and A chain of activated two chain uPA were detected by rabbit anti-uPA antibody recognizing all three uPA species. Position of molecular weight markers is indicated in kDa on the left. **C:** Contribution of uPA activation and activity to PC-hi/diss intravasation. Developing PC-hi/diss CAM tumors were treated topically with control IgG, mAb-112, mAb-2, or aprotinin. After 7 days, primary tumors were weighed (**left graph**) and intravasation to the distal CAM was quantified by *Alu*-qPCR (**right graph**). Presented are means ± SEM from pooled data of three independent experiments using from 22 to 53 embryos per variable. The levels of intravasation are presented as percentage of intravasation determined in the IgG-treated control. **D:** Contribution of uPA to Matrigel invasion in Transwells. PC-lo/diss or PC-hi/diss cells were stimulated to invade Matrigel toward CM from CEFs. Where indicated, mAb-112 or aprotinin were added to both inner and outer chambers. Presented are means ± SEM from pooled data of three independent experiments performed in duplicate. Data are calculated as percentage of invasion observed in control IgG-treated PC-hi/diss variant. **E:** Contribution of uPA to CAM angiogenesis. Collagen onplants containing PC-lo/diss cells mixed with control IgG and PC-hi/diss cells mixed with control IgG, mAb-112, or aprotinin were placed onto the CAMs of shell-less chick embryos. The scattergram depicts angiogenic indices in individual collagen onplants from a representative experiment scored at 72 hours; lines are means. $^{*}P < 0.05$, $^{**}P < 0.005$, and $^{***}P < 0.001$ in two-tailed Student's *t*-test; $^{\#}P < 0.05$ in one-tailed Student's *t*-test.

we have linked increased tumor angiogenesis with the increased dissemination capability of PC-hi/diss, we analyzed the contributions of uPA to PC-hi/diss angiogenesis in the CAM collagen onplant model. Incorporation of function-blocking mAb-112 or aprotinin into collagen

grafts containing PC-hi/diss cells, significantly decreased tumor-induced angiogenesis by 50% and 75%, respectively (Figure 7E). Thus, uPA appears to significantly contribute to PC-hi/diss intravasation and metastasis via multiple mechanisms, namely by facilitating tumor angiogenesis and tissue invasion.

Discussion

Because the multistep metastatic cascade involves complex interactions between tumor cells and stromal cells, tumor-associated vasculature and extracellular matrix components, the study of this process requires *in vivo* analyses. Therefore, the development of easily manipulatable *in vivo* models greatly facilitates metastasis investigations.[27–30] Further dissection of individual rate-limiting processes by *in vitro* and *in vivo* modeling is also necessary to define the molecular and cellular mechanisms that lead to successful tumor cell dissemination. Intravasation, ie, the entry of aggressive cells into the vasculature, is an early and very much understudied rate-limiting step in the metastatic cascade.[31,32] To identify specific processes and molecules that functionally contribute to tumor cell intravasation, our laboratory has generated pairs of congenic tumor cell lines differing substantially in their intravasation potentials, namely the HT-1080 fibrosarcoma variants characterized previously,[9,11–13] and prostate carcinoma PC-3 cell variants described herein.

The PC-3 variants, ie, PC-lo/diss and PC-hi/diss, differ by an average of 40-fold in their ability to disseminate in the chick embryo spontaneous metastasis model, while exhibiting similar capacity to colonize the CAM after i.v. inoculation, indicating that the two PC-3 variants specifically differ during early metastatic events leading to intravasation. This difference does not appear to be dependent on tumor weight, as a retrospective analysis of embryos bearing tumors of the same size revealed a consistent differential (up to 100-fold) in intravasation. Therefore, a comparative analysis of the PC-hi/diss and PC-lo/diss cell variants provides a valuable means to investigate critical determinants of intravasation.

It is important that in addition to the differences manifested in the chick embryo model, the PC-3 cell dissemination variants also exhibited differential abilities to metastasize in two murine model systems, a renal capsule model and an orthotopic model. The kidney cortex provides a rich vascular microenvironment amenable to rapid growth and hematogenous dissemination of implanted tumor cells.[33–35] In this model, PC-hi/diss and PC-lo/diss cells formed sizable primary tumors within 3–4 weeks on grafting under the renal capsule, but PC-hi/diss bearing animals presented more extensive metastases to the liver and lung. Xenotransplantation of tumor cells into the appropriate anatomical location has been shown to affect gene expression and increase tumor growth rate and metastasis, as compared with nonorthotopic sites, especially subcutaneous implants.[36,37] While both PC-3 cell variants gave rise to large primary tumors in the orthotopic site within 4 to 6 weeks, PC-hi/diss cells more efficiently metastasized to lymph nodes, liver, lungs, and spleen of recipient mice. Lymph nodes were visibly enlarged and contained more human tumor cells per million host cells than any other organ examined, consistent with the usual pattern of carcinoma lymphatic dissemination before widespread hematogenous dissemination.[38,39] Additionally, mice bearing PC-hi/diss tumors developed large volume tumor cell ascites in the peritoneal cavity and multiple macroscopic foci of tumor cells on the mesenterium. It could be argued that the peritoneal ascites, and not vascular or lymphatic dissemination, might be a source of secondary metastases, especially those in the liver. However, colonies of PC-hi/diss tumor cells were repeatedly found within the lung parenchyma by histological analyses, indicating that these tumor cells metastasized via a hematogenous route to reach and colonize the lungs, which are not directly accessible to tumor cells in peritoneal ascites.

The large differential in spontaneous dissemination demonstrated by PC-hi/diss and PC-lo/diss congenic cell variants both in the chick embryo and mouse models, facilitated an identification of key processes and molecules underlying the early events in metastasis. Tumor angiogenesis has long been correlated with aggressive prostate cancer and metastasis,[40] although it remains to be determined conclusively whether the angiogenic vessels serve as the actual primary conduits for direct tumor cell intravasation instead of the more stable pre-existing vasculature. Correlating with an increased dissemination potential, the PC-hi/diss cell variant displayed an enhanced ability to induce angiogenesis in avian and murine hosts. PC-hi/diss also manifested a significant increase in VEGF production. A function-blocking antibody to VEGF significantly inhibited PC-hi/diss tumor angiogenesis in the avian angiogenesis model, suggesting that the increase in VEGF secretion functionally contributes to PC-hi/diss-induced angiogenesis. When the anti-VEGF antibody was applied to developing PC-hi/diss primary CAM tumors, the treatment concomitantly reduced vessel density within the tumors and significantly decreased intravasation. Importantly, the anti-VEGF treatment did not significantly affect tumor growth in the chick embryo. In murine models, anti-angiogenic treatments primarily affect tumor growth and secondarily metastatic dissemination. Moreover, reduced primary tumor size makes it difficult to determine direct effects of anti-angiogenic treatment on tumor metastasis.[41,42] In the CAM model, on the other hand, it appears that the intratumoral angiogenic vessels, remaining after anti-VEGF treatment along with the pre-existing CAM blood vessels, are able to sustain normal tumor growth without onset of hypoxia or significant reduction in tumor size. This suggests that decreasing the number of intratumoral angiogenic vessels directly limits the number of vascular points of entry available to the escaping tumor cells. Furthermore, these findings highlight a unique aspect of the chick embryo metastasis model, in which the confounding factor of reduced tumor size indirectly contributing to reduction of metastasis is reduced or can be eliminated.

Before reaching blood vessels, tumor cells are believed to actively escape from the primary tumor and invade surrounding stromal tissues. In epithelial-derived

tumors, EMT may be involved in facilitating tumor cell escape.[43,44] EMT, originally described and characterized in development, has been recently implicated in cancer progression as several morphological characteristics and protein expression changes are seen in both developmental EMT and cancer metastasis.[17,18] EMT in development and possibly in cancer progression can be mediated by a group of transcription factors (ie, Snail, Slug, and Twist) that, when activated, induce phenotypic changes in cell behavior.[19,20,45,46] These changes involve a loss of polarity and loosening of tight cell–cell junctions, coinciding with decreased levels of functional epithelial markers, especially E-cadherin. A gain of mesenchymal characteristics is also observed, including increased motility and expression of mesenchymal markers (N-cadherin, vimentin, fibronectin). Full or partial EMT is believed to enable aggressive cells to escape from the primary site and this process has been associated with enhanced metastatic potential. EMT in cancer is not as well understood as the parallel process during embryonic development, and the occurrence of EMT in cancer progression remains controversial and requires further definition.[47–49]

In the current study, we observed a substantial loss of E-cadherin expression in PC-hi/diss, however N-cadherin was expressed by both PC-lo/diss and PC-hi/diss and there was no detectable expression of vimentin in either variant. The transcription factors Snail, Slug, and Twist were also detected at similar levels between the two variants. This is in contrast to studies on breast carcinoma showing that these transcription factors repress E-cadherin expression, or conversely, that E-cadherin repression leads to up-regulation of Snail, Slug, and Twist.[50] Thus, our data suggests that these factors may play different roles in different carcinoma cell types. Additionally, due to dysfunctional components of the catenin pathway in the PC-3 cell line,[51,52] it is unclear whether the loss of E-cadherin would be a prerequisite for efficient intravasation of PC-hi/diss. Altogether, despite the clear loss of E-cadherin expression, the intravasating phenotype of PC-hi/diss does not appear to be adequately explained by a full or partial EMT.

Serine proteases, especially uPA, have been implicated in prostate carcinoma progression both by clinical biopsy association studies, indicating elevated uPA expression and secretion in high-grade prostate carcinomas,[24,53–56] and in preclinical animal models, where siRNA to uPA decreases tumor growth and metastasis of prostate carcinoma cell lines.[57,58] In the chick embryo model, blocking uPA has been previously shown to dampen metastasis of the human epidermoid HEp-3 carcinoma.[8] Recently, by chemical proteomic and functional analyses, we were able to directly implicate uPA activation in the process of HT-1080 tumor cell intravasation.[11,14] The observed enhancement in dissemination and *in vitro* invasion ability of PC-hi/diss led us to analyze a potential role of uPA in PC-hi/diss dissemination. The PC-hi/diss cells secrete more uPA protein, which is present in the CM as both the single chain zymogen and the two-chain, disulfide-linked, activated enzyme. To determine the functional significance of this differential, we modulated uPA activation and activity in PC-hi/diss *in vitro* and *in vivo*. One relatively under-explored mechanism for interfering with protease function is by preventing zymogen activation.[14] Function-blocking mAb-112, which inhibits activation of uPA zymogen, has demonstrated anti-intravasation function in a fibrosarcoma model.[14] In the current study, we have confirmed the efficacy of preventing uPA activation as a strategy to inhibit intravasation, expanding our previous findings to a carcinoma model system. Specifically targeting zymogen activation of uPA with mAb-112 was as effective as blocking uPA activity using an independent function-blocking antibody, mAb-2.

The broad-spectrum serine protease inhibitor, aprotinin, also substantially inhibited intravasation. Although aprotinin does not directly target uPA, it is a potent inhibitor of plasmin, a major feed-back activator of pro-uPA *in vivo* as well as a key product generated by uPA activation of plasminogen. Therefore, inhibition of PC-hi/diss intravasation by aprotinin strongly implicates the uPA/plasmin system in the early processes of metastatic spread. Treatments with mAb-112 and aprotinin significantly decreased Matrigel invasion of PC-hi/diss cells *in vitro*, suggesting that the enhanced invasion might be a possible mechanism by which active uPA could contribute to PC-hi/diss intravasation. Despite the fact that uPA can have plasmin-independent functions via interactions with uPAR and other cell surface molecules,[26,59–61] the near-complete blockade of intravasation by aprotinin suggests that uPA likely functions via plasmin in the PC-hi/diss system.

In addition to the classical role of ECM remodeling and invasion,[24–26,62] uPA and plasmin have been linked to tumor angiogenesis by directly facilitating endothelial cell migration and invasion[61] and by releasing angiogenic growth factors, including VEGF, from the extracellular matrix.[25,63] Since we have shown that dampening angiogenesis via anti-VEGF treatment can decrease intravasation, we asked whether active uPA might also contribute to intravasation by an angiogenic mechanism. Indeed, when mAb-112 or aprotinin were incorporated into PC-hi/diss containing collagen onplants and angiogenesis was scored, both approaches, ie, inhibiting uPA activation and blocking serine protease activity, substantially decreased PC-hi/diss tumor angiogenesis. Thus, it appears that interfering with uPA activation and activity might block intravasation/metastasis by at least two separate mechanisms: 1) decreasing ECM invasion and 2) decreasing tumor angiogenesis. Intriguingly, recent studies have reported that disrupting the tumor vasculature alone can actually *increase* the invasive behavior of tumor cells[64–67] due to hypoxia-response programs.[68] Although we did not observe any increase in tumor cell intravasation after anti-VEGF treatment, the possibility of dampening both invasion and angiogenesis simultaneously via targeting a protease pathway could be one potential way to overcome the problem of possible increased tumor invasiveness after anti-angiogenic treatment.

In conclusion, we have successfully generated a novel pair of prostate carcinoma PC-3 dissemination variants that differ substantially in their capacity to complete early steps of the metastatic cascade that culminate in intra-

vasation. A comparative analysis of these congenic variants has indicated important functional roles for VEGF secretion and uPA activation in facilitating tumor cell intravasation and has indicated a potential direct link between tumor-induced angiogenesis and tumor cell intravasation.

Acknowledgments

We thank Chenxing Li for her excellent technical assistance.

References

1. Naito S, Walker SM, Fidler IJ: In vivo selection of human renal cell carcinoma cells with high metastatic potential in nude mice. Clin Exp Metastasis 1989, 7:381–389
2. Vezeridis MP, Tzanakakis GN, Meitner PA, Doremus CM, Tibbetts LM, Calabresi P: In vivo selection of a highly metastatic cell line from a human pancreatic carcinoma in the nude mouse. Cancer 1992, 69:2060–2063
3. Pettaway CA, Pathak S, Greene G, Ramirez E, Wilson MR, Killion JJ, Fidler IJ: Selection of highly metastatic variants of different human prostatic carcinomas using orthotopic implantation in nude mice. Clin Cancer Res 1996, 2:1627–1636
4. Morikawa K, Walker SM, Jessup JM, Fidler IJ: In vivo selection of highly metastatic cells from surgical specimens of different primary human colon carcinomas implanted into nude mice. Cancer Res 1988, 48:1943–1948
5. Kang Y, Siegel PM, Shu W, Drobnjak M, Kakonen SM, Cordon-Cardo C, Guise TA, Massague J: A multigenic program mediating breast cancer metastasis to bone. Cancer Cell 2003, 3:537–549
6. Nicholson BE, Frierson HF, Conaway MR, Seraj JM, Harding MA, Hampton GM, Theodorescu D: Profiling the evolution of human metastatic bladder cancer. Cancer Res 2004, 64:7813–7821
7. Minn AJ, Kang Y, Serganova I, Gupta GP, Giri DD, Doubrovin M, Ponomarev V, Gerald WL, Blasberg R, Massague J: Distinct organ-specific metastatic potential of individual breast cancer cells and primary tumors. J Clin Invest 2005, 115:44–55
8. Kim J, Yu W, Kovalski K, Ossowski L: Requirement for specific proteases in cancer cell intravasation as revealed by a novel semiquantitative PCR-based assay. Cell 1998, 94:353–362
9. Deryugina EI, Zijlstra A, Partridge JJ, Kupriyanova TA, Madsen MA, Papagiannakopoulos T, Quigley JP: Unexpected effect of matrix metalloproteinase down-regulation on vascular intravasation and metastasis of human fibrosarcoma cells selected in vivo for high rates of dissemination. Cancer Res 2005, 65:10959–10969
10. Zijlstra A, Mellor R, Panzarella G, Aimes RT, Hooper JD, Marchenko ND, Quigley JP: A quantitative analysis of rate-limiting steps in the metastatic cascade using human-specific real-time polymerase chain reaction. Cancer Res 2002, 62:7083–7092
11. Madsen MA, Deryugina EI, Niessen S, Cravatt BF, Quigley JP: Activity-based protein profiling implicates urokinase activation as a key step in human fibrosarcoma intravasation. J Biol Chem 2006, 281:15997–16005
12. Partridge JJ, Madsen MA, Ardi VC, Papagiannakopoulos T, Kupriyanova TA, Quigley JP, Deryugina EI: Functional analysis of matrix metalloproteinases and tissue inhibitors of metalloproteinases differentially expressed by variants of human HT-1080 fibrosarcoma exhibiting high and low levels of intravasation and metastasis. J Biol Chem 2007, 282:35964–35977
13. Conn EM, Madsen MA, Cravatt BF, Ruf W, Deryugina EI, Quigley JP: Cell surface proteomics identifies molecules functionally linked to tumor cell intravasation. J Biol Chem 2008, 283:26518–26527
14. Blouse GE, Botkjaer KA, Deryugina E, Byszuk AA, Jensen JM, Mortensen KK, Quigley JP, Andreasen PA: A novel mode of intervention with serine protease activity: targeting zymogen activation. J Biol Chem 2009, 284:4647–4657
15. Deryugina EI, Quigley JP: Chapter 2. Chick embryo chorioallantoic membrane models to quantify angiogenesis induced by inflammatory and tumor cells or purified effector molecules. Methods Enzymol 2008, 444:21–41
16. Ardi VC, Kupriyanova TA, Deryugina EI, Quigley JP: Human neutrophils uniquely release TIMP-free MMP-9 to provide a potent catalytic stimulator of angiogenesis. Proc Natl Acad Sci USA 2007, 104:20262–20267
17. Thiery JP, Sleeman JP: Complex networks orchestrate epithelial-mesenchymal transitions. Nat Rev Mol Cell Biol 2006, 7:131–142
18. Yang J, Weinberg RA: Epithelial-mesenchymal transition: at the crossroads of development and tumor metastasis. Dev Cell 2008, 14:818–829
19. Moreno-Bueno G, Portillo F, Cano A: Transcriptional regulation of cell polarity in EMT and cancer. Oncogene 2008, 27:6958–6969
20. Yang J, Mani SA, Weinberg RA: Exploring a new twist on tumor metastasis. Cancer Res 2006, 66:4549–4552
21. Duffy MJ, McGowan PM, Gallagher WM: Cancer invasion and metastasis: changing views. J Pathol 2008, 214:283–293
22. Ludwig T: Local proteolytic activity in tumor cell invasion and metastasis. Bioessays 2005, 27:1181–1191
23. Egeblad M, Werb Z: New functions for the matrix metalloproteinases in cancer progression. Nat Rev Cancer 2002, 2:161–174
24. Li Y, Cozzi PJ: Targeting uPA/uPAR in prostate cancer. Cancer Treat Rev 2007, 33:521–527
25. Duffy MJ: The urokinase plasminogen activator system: role in malignancy. Curr Pharm Des 2004, 10:39–49
26. Andreasen PA, Egelund R, Petersen HH: The plasminogen activation system in tumor growth, invasion, and metastasis. Cell Mol Life Sci 2000, 57:25–40
27. Gupta GP, Massague J: Cancer metastasis: building a framework. Cell 2006, 127:679–695
28. Fidler IJ, Kim SJ, Langley RR: The role of the organ microenvironment in the biology and therapy of cancer metastasis. J Cell Biochem 2007, 101:927–936
29. Kopfstein L, Christofori G: Metastasis: cell-autonomous mechanisms versus contributions by the tumor microenvironment. Cell Mol Life Sci 2006, 63:449–468
30. Chambers AF, Groom AC, MacDonald IC: Dissemination and growth of cancer cells in metastatic sites. Nat Rev Cancer 2002, 2:563–572
31. Wyckoff JB, Jones JG, Condeelis JS, Segall JE: A critical step in metastasis: in vivo analysis of intravasation at the primary tumor. Cancer Res 2000, 60:2504–2511
32. Wyckoff JB, Wang Y, Lin EY, Li JF, Goswami S, Stanley ER, Segall JE, Pollard JW, Condeelis J: Direct visualization of macrophage-assisted tumor cell intravasation in mammary tumors. Cancer Res 2007, 67:2649–2656
33. Bennett JA, Pilon VA, MacDowell RT: Evaluation of growth and histology of human tumor xenografts implanted under the renal capsule of immunocompetent and immunodeficient mice. Cancer Res 1985, 45:4963–4969
34. Wang Y, Revelo MP, Sudilovsky D, Cao M, Chen WG, Goetz L, Xue H, Sadar M, Shappell SB, Cunha GR, Hayward SW: Development and characterization of efficient xenograft models for benign and malignant human prostate tissue. Prostate 2005, 64:149–159
35. Lee CH, Xue H, Sutcliffe M, Gout PW, Huntsman DG, Miller DM, Gilks CB, Wang YZ: Establishment of subrenal capsule xenografts of primary human ovarian tumors in SCID mice: potential models. Gynecol Oncol 2005, 96:48–55
36. Killion JJ, Radinsky R, Fidler IJ: Orthotopic models are necessary to predict therapy of transplantable tumors in mice. Cancer Metastasis Rev 1998, 17:279–284
37. Nakamura T, Fidler IJ, Coombes KR: Gene expression profile of metastatic human pancreatic cancer cells depends on the organ microenvironment. Cancer Res 2007, 67:139–148
38. Bubendorf L, Schopfer A, Wagner U, Sauter G, Moch H, Willi N, Gasser TC, Mihatsch MJ: Metastatic patterns of prostate cancer: an autopsy study of 1,589 patients. Hum Pathol 2000, 31:578–583
39. Wong SY, Hynes RO: Lymphatic or hematogenous dissemination: how does a metastatic tumor cell decide? Cell Cycle 2006, 5:812–817
40. Weidner N, Carroll PR, Flax J, Blumenfeld W, Folkman J: Tumor angiogenesis correlates with metastasis in invasive prostate carcinoma. Am J Pathol 1993, 143:401–409
41. Loges S, Mazzone M, Hohensinner P, Carmeliet P: Silencing or fuel-

ing metastasis with VEGF inhibitors: antiangiogenesis revisited. Cancer Cell 2009, 15:167–170
42. Ferrara N, Kerbel RS: Angiogenesis as a therapeutic target. Nature 2005, 438:967–974
43. Blick T, Widodo E, Hugo H, Waltham M, Lenburg ME, Neve RM, Thompson EW: Epithelial mesenchymal transition traits in human breast cancer cell lines. Clin Exp Metastasis 2008, 25:629–642
44. Berx G, Raspe E, Christofori G, Thiery JP, Sleeman JP: Pre-EMTing metastasis? Recapitulation of morphogenetic processes in cancer. Clin Exp Metastasis 2007, 24:587–597
45. Savagner P: Leaving the neighborhood: molecular mechanisms involved during epithelial-mesenchymal transition. Bioessays 2001, 23:912–923
46. Olmeda D, Montes A, Moreno-Bueno G, Flores JM, Portillo F, Cano A: Snai1 and Snai2 collaborate on tumor growth and metastasis properties of mouse skin carcinoma cell lines. Oncogene 2008, 27:4690–4701
47. Tarin D, Thompson EW, Newgreen DF: The fallacy of epithelial mesenchymal transition in neoplasia, Cancer Res 2005, 65:5996–6000; discussion 6000–5991
48. Christiansen JJ, Rajasekaran AK: Reassessing epithelial to mesenchymal transition as a prerequisite for carcinoma invasion and metastasis. Cancer Res 2006, 66:8319–8326
49. Thompson EW, Newgreen DF, Tarin D: Carcinoma invasion and metastasis: a role for epithelial-mesenchymal transition? Cancer Res 2005, 65:5991–5995; discussion 5995
50. Onder TT, Gupta PB, Mani SA, Yang J, Lander ES, Weinberg RA: Loss of E-cadherin promotes metastasis via multiple downstream transcriptional pathways. Cancer Res 2008, 68:3645–3654
51. Morton RA, Ewing CM, Nagafuchi A, Tsukita S, Isaacs WB: Reduction of E-cadherin levels and deletion of the alpha-catenin gene in human prostate cancer cells. Cancer Res 1993, 53:3585–3590
52. Ewing CM, Ru N, Morton RA, Robinson JC, Wheelock MJ, Johnson KR, Barrett JC, Isaacs WB: Chromosome 5 suppresses tumorigenicity of PC3 prostate cancer cells: correlation with re-expression of alpha-catenin and restoration of E-cadherin function. Cancer Res 1995, 55:4813–4817
53. Van Veldhuizen PJ, Sadasivan R, Cherian R, Wyatt A: Urokinase-type plasminogen activator expression in human prostate carcinomas. Am J Med Sci 1996, 312:8–11
54. Shariat SF, Roehrborn CG, McConnell JD, Park S, Alam N, Wheeler TM, Slawin KM: Association of the circulating levels of the urokinase system of plasminogen activation with the presence of prostate cancer and invasion, progression, and metastasis. J Clin Oncol 2007, 25:349–355
55. Cozzi PJ, Wang J, Delprado W, Madigan MC, Fairy S, Russell PJ, Li Y: Evaluation of urokinase plasminogen activator and its receptor in different grades of human prostate cancer. Hum Pathol 2006, 37: 1442–1451
56. Miyake H, Hara I, Yamanaka K, Gohji K, Arakawa S, Kamidono S: Elevation of serum levels of urokinase-type plasminogen activator and its receptor is associated with disease progression and prognosis in patients with prostate cancer. Prostate 1999, 39:123–129
57. Pulukuri SM, Gondi CS, Lakka SS, Jutla A, Estes N, Gujrati M, Rao JS: RNA interference-directed knockdown of urokinase plasminogen activator and urokinase plasminogen activator receptor inhibits prostate cancer cell invasion, survival, and tumorigenicity in vivo. J Biol Chem 2005, 280:36529–36540
58. Pulukuri SM, Rao JS: Small interfering RNA directed reversal of urokinase plasminogen activator demethylation inhibits prostate tumor growth and metastasis. Cancer Res 2007, 67:6637–6646
59. Blasi F, Carmeliet P: uPAR: a versatile signalling orchestrator. Nat Rev Mol Cell Biol 2002, 3:932–943
60. Sidenius N, Blasi F: The urokinase plasminogen activator system in cancer: recent advances and implication for prognosis and therapy. Cancer Metastasis Rev 2003, 22:205–222
61. Binder BR, Mihaly J, Prager GW: uPAR-uPA-PAI-1 interactions and signaling: a vascular biologist's view. Thromb Haemost 2007, 97: 336–342
62. Dano K, Behrendt N, Hoyer-Hansen G, Johnsen M, Lund LR, Ploug M, Romer J: Plasminogen activation and cancer. Thromb Haemost 2005, 93:676–681
63. Park JE, Keller GA, Ferrara N: The vascular endothelial growth factor (VEGF) isoforms: differential deposition into the subepithelial extracellular matrix and bioactivity of extracellular matrix-bound VEGF. Mol Biol Cell 1993, 4:1317–1326
64. Kunkel P, Ulbricht U, Bohlen P, Brockmann MA, Fillbrandt R, Stavrou D, Westphal M, Lamszus K: Inhibition of glioma angiogenesis and growth in vivo by systemic treatment with a monoclonal antibody against vascular endothelial growth factor receptor-2. Cancer Res 2001, 61:6624–6628
65. Paez-Ribes M, Allen E, Hudock J, Takeda T, Okuyama H, Vinals F, Inoue M, Bergers G, Hanahan D, Casanovas O: Antiangiogenic therapy elicits malignant progression of tumors to increased local invasion and distant metastasis. Cancer Cell 2009, 15:220–231
66. Du R, Lu KV, Petritsch C, Liu P, Ganss R, Passegue E, Song H, Vandenberg S, Johnson RS, Werb Z, Bergers G: HIF1alpha induces the recruitment of bone marrow-derived vascular modulatory cells to regulate tumor angiogenesis and invasion. Cancer Cell 2008, 13:206–220
67. Ebos JM, Lee CR, Cruz-Munoz W, Bjarnason GA, Christensen JG, Kerbel RS: Accelerated metastasis after short-term treatment with a potent inhibitor of tumor angiogenesis. Cancer Cell 2009, 15:232–239
68. Brahimi-Horn MC, Chiche J, Pouyssegur J: Hypoxia and cancer. J Mol Med 2007, 85:1301–1307